

Article

DNAzymes-Embedded Framework Nucleic Acids (FNAzymes) for Metal Ions Imaging in Living Cells

Dan Zhu ¹, Jiakuan Huang ¹, Yanting Xia ¹, Shao Su ¹ , Xiaolei Zuo ^{2,3}, Qian Li ^{2,*} and Lianhui Wang ^{1,*}

¹ State Key Laboratory of Organic Electronics and Information Displays & Jiangsu Key Laboratory for Biosensors, Institute of Advanced Materials (IAM), Nanjing University of Posts and Telecommunications, Nanjing 210023, China; iamdzhu@njupt.edu.cn (D.Z.); iamjxhuang@163.com (J.H.); iamytxia@163.com (Y.X.); iamssu@njupt.edu.cn (S.S.)

² School of Chemistry and Chemical Engineering, National Center for Translational Medicine, Shanghai Jiao Tong University, Shanghai 200240, China; zuoxiaolei@sjtu.edu.cn

³ Shanghai Key Laboratory for Nucleic Acids Chemistry and Nanomedicine, Institute of Molecular Medicine, Renji Hospital, School of Medicine, Shanghai Jiao Tong University, Shanghai 200127, China

* Correspondence: liqian2018@sjtu.edu.cn (Q.L.); iamlhwan@njupt.edu.cn (L.W.)

Abstract: Simultaneous and non-destructive quantitative detection of intracellular metal ions holds great promise for improving the accuracy of diagnosis and biological research. Herein, novel multicolor DNAzymes-embedded framework nucleic acids (FNAzymes) were presented, which can easily enter cells and achieve simultaneous and quantitative detection of intracellular physiologically related Cu^{2+} and Zn^{2+} . Two types of DNAzymes, specific to Cu^{2+} and Zn^{2+} , were encoded in the framework nucleic acids (FNAs) via self-assembly. With the formation of a well-ordered FNAzyme nanostructure, the fluorophore and the quencher were close to each other; therefore, the fluorescence was quenched. In the presence of Cu^{2+} and Zn^{2+} , the integrated FNAzymes would be specifically cleaved, resulting in the release of fluorophores in cells. Consequently, the fluorescence in living cells could be observed by a confocal microscope and semi-quantitatively analyzed by flow cytometry with low-nanomolar sensitivity for both metal ions. The FNAzymes have high uniformity and structural accuracy, which are beneficial for intracellular detection with excellent reproducibility. This proposed method offers new opportunities for non-destructive, semi-quantitative, multi-target detection in living cells.

Keywords: Framework Nucleic Acids (FNAs); DNAzyme; metal ions; intracellular imaging; flow cytometry



Citation: Zhu, D.; Huang, J.; Xia, Y.; Su, S.; Zuo, X.; Li, Q.; Wang, L. DNAzymes-Embedded Framework Nucleic Acids (FNAzymes) for Metal Ions Imaging in Living Cells.

Chemosensors **2023**, *11*, 358.

<https://doi.org/10.3390/chemosensors11070358>

[chemosensors11070358](https://doi.org/10.3390/chemosensors11070358)

Academic Editor: Chunsheng Wu

Received: 25 May 2023

Revised: 20 June 2023

Accepted: 23 June 2023

Published: 25 June 2023



Copyright: © 2023 by the authors. Licensee MDPI, Basel, Switzerland. This article is an open access article distributed under the terms and conditions of the Creative Commons Attribution (CC BY) license (<https://creativecommons.org/licenses/by/4.0/>).

1. Introduction

Physiologically related metal ions play a significant role in regulating cellular functions and life activities [1]. Among these ions, Cu^{2+} and Zn^{2+} are the second and third most abundant transition metal ions (after Fe^{3+}) inside the human body, and they participate in a variety of intra- and extracellular physiological processes, such as neural signal transmission, cellular metabolism, and respiration [2,3]. An increasing number of studies have demonstrated that the concentrations of Cu^{2+} and Zn^{2+} in vivo are correlated with many nutrition-related or enzyme-related diseases, such as genetic disorders, epilepsy, Parkinson's disease, and even cancers [4]. For instance, the relative concentration ratio of $\text{Cu}^{2+}/\text{Zn}^{2+}$ has been considered to be an important indicator for numerous diseases, such as colorectal cancer, lung cancer, and relapsing-remitting multiple sclerosis [5]. In the cell signaling pathway, Cu^{2+} and Zn^{2+} always function complementarily to each other to regulate biological processes [6]. Therefore, quantitative detection of Zn^{2+} and Cu^{2+} simultaneously at the cellular level holds great hope for better understanding the working mechanisms of physiologically related metal ions in biological processes and has potential in biomedical applications.

The most widely used methods for conventional quantitative detection of metal elements involve inductively coupled plasma-mass spectrometry (ICP-MS) [7], inductively coupled plasma-atomic emission spectrometry (ICP-AES) [8], and atomic absorption spectrometry (AAS) [9]. These methods are commonly cumbersome and cell-destructive, and thus, they are not suitable for live-cell detection. In recent years, fluorescent sensors have turned out to be powerful tools for intracellular and super-resolution imaging [10–12]. Great efforts have been focused on the development of fluorescent probes for the imaging of intracellular metal ions such as Ca^{2+} , Cu^{2+} , Zn^{2+} , and Mg^{2+} [13–15]. Nevertheless, tedious organic synthesis steps are often required to fabricate these probes. Most small molecule probe-based approaches can only detect an individual ion due to their limited specificity towards metal ions, which restricts their applications in multiple detections. Therefore, it developing effective techniques for the non-destructive quantitative determination of multiple metal ions in living cells with high sensitivity and selectivity is in high demand.

DNAzymes are a class of functional nucleic acids that exhibit catalytic activity in the presence of specific targets [16,17]. The biocompatibility, low cytotoxicity, and ease of coding allow DNAzymes to be a powerful tool for intracellular analysis. Numerous DNAzymes specific for various metal ions (such as Na^+ , Pb^{2+} , UO_2^{2+} , and K^+) have been selected for sensitive detection *in vitro* and *in vivo* [18,19]. However, due to the simple structure and the existing RNA site, DNAzymes are vulnerable to nucleases in the cell environment. To increase the stability of DNAzyme in living cells, nanocarriers have been used to assist the transfer of DNAzyme into cells, such as gold nanoparticles, two-dimensional nanomaterials, and polymers [20–22]. However, these assays also suffer from some inherent limitations. For instance, the sizes of carriers, the number of signaling molecules on carriers, and the carriers themselves could vary among different batches. Additionally, multiple-step modifications of small molecules (such as thiolated probes, fluorescent probes, or other probes) exacerbate the inhomogeneity between probes. Considering the complexity of the intracellular environment, developing probes with high uniformity and structural precision is urgent for improving the accuracy of quantification in living cells. Self-assembled framework nucleic acids (FNAs) are nano-functional materials constructed by several DNA strands through highly specific base-pairing, which have aroused widespread concern due to their ease of designing, low cytotoxicity, and good stability [23–25]. Compared to other nanocarriers, FNAs have high uniformity and structural accuracy, which is beneficial for detection with excellent repeatability [26–28]. It has been demonstrated that FNAs could penetrate cell membranes by a caveolin-dependent pathway without the assistance of transfection agents and maintain good stability in living cells, which allows FNAs to be powerful nanocarriers for intracellular applications [29].

In this work, we designed DNAzymes-embedded framework nucleic acids (FNAzymes) for the simultaneous semi-quantitative determination and imaging of intracellular Cu^{2+} and Zn^{2+} . Cu^{2+} -specific DNAzymes [30] and Zn^{2+} -specific DNAzymes [31] were employed as recognition elements, and tetrahedral FNAs were used as nanocarriers for cellular transport (Figure 1A). Benefiting from the high structural uniformity of FNAs, the incorporation of DNAzymes with FNAs might provide a platform for intracellular detection with enhanced precision. The fluorescence inside cells was observed using a laser scanning confocal microscope (LSCM). The fluorescence was analyzed using flow cytometry, which allowed for the semi-quantitative determination of intracellular metal ions (Figure 1B).

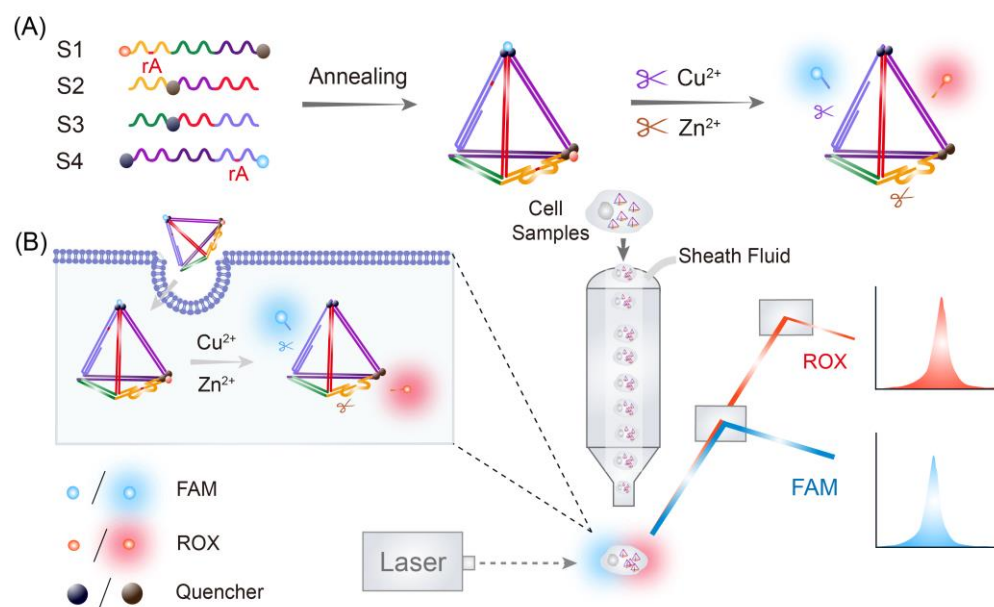


Figure 1. (A) Scheme of the assembly and metal ions in response to the multifunctional tetrahedral DNA nanostructure-based nanoprobe with embedded DNAzymes (FNAzymes). (B) The simultaneous intracellular semi-quantification of Cu²⁺ and Zn²⁺ by flow cytometer.

2. Materials and Methods

2.1. Chemicals

DNA samples (listed in Table S1) were synthesized by TaKaRa Inc. (Dalian, China). Tris (hydroxymethyl) aminomethane (Tris), NaCl, KCl, CaCl₂, Cu(CH₃COO)₂·H₂O, Zn(CH₃COO)₂·2H₂O, FeCl₃, Mn(CH₃COO)₂·4H₂O, MgCl₂·6H₂O, Cd(NO₃)₂·6H₂O, NiSO₄·6(H₂O), Co(CH₃COO)₂·4H₂O, and diethylpyrocarbonate (DEPC) were purchased from China National Sinopharm Chemical Reagent Co., Ltd. (Shanghai, China). Human cervical cancer cell line (HeLa) was purchased from Jiangsu Keygen Biotech Corp. Ltd. (Nanjing, China). Additionally, 3-(4,5-Dimethylthiazol-2-yl)-2,5-diphenyltetrazolium bromide (MTT) was purchased from Sigma-Aldrich (St. Louis, MO, USA). All solutions were treated with DEPC-treated ultrapure water to prevent RNA degradation by RNA enzyme. Buffer A: 20 mM Tris-HCl, 50 mM MgCl₂, pH 8.0. Buffer B: 50 mM Tris-HCl, 100 mM NaCl, 2 mM MgCl₂, pH 7.4.

2.2. Assembly of Multifunctional FNAzymes

The FNAzymes were prepared by adding the four DNA strands (strands S1–S4) in equimolar quantities together in buffer A. The solution was heated to 95 °C for 10 min, followed by rapid cooling to 4 °C. The FNAzymes were loaded onto an 8% polyacrylamide gel electrophoresis (PAGE, 8%) and imaged using a GBOX-F3-E system (Syngene UK, Massachusetts, England). The prepared FNAzymes were stored at 4 °C for further use.

2.3. AFM Imaging

The FNAzymes were diluted to 20 nM with Buffer A. Subsequently, 40 µL of APTES (0.5%) was incubated on freshly cleaved mica for a duration of 5 min. Following this, the mica surface was rinsed with Milli-Q water and dried using N₂ gas. Next, 10 µL of 20 nM FNAzymes were incubated on the treated mica for 5 min. After thorough washing, the assembly buffer was added to reach a final volume of 100 µL. The sample was then subjected to scanning using a Jscanner attached to a Multimode NanoscopeIIIa AFM (Veeco/Digital Instruments) operating in peak force mode.

2.4. Simultaneous Detection of Cu^{2+} and Zn^{2+} In Vitro

FNAzymes were firstly diluted to a concentration of 50 nM in buffer B. Various concentrations of Cu^{2+} and Zn^{2+} were then added and allowed to incubate together at 37 °C for 20 min. Fluorescence intensity of samples was recorded by RF-5301PC (Shimadzu, Tokyo, Japan). For FAM, the excitation wavelength was 494 nm, and the fluorescence spectrum was collected from 505 to 600 nm. For ROX, the excitation wavelength was 580 nm, and the fluorescence spectrum was collected from 595 to 660 nm.

2.5. Stability of FNAzymes

The FNAzymes were concentrated to 1 μM in 5 U/L of DNase I or 50% cell lysate and incubated at 37 °C. The samples collected at different time points were characterized by 8% PAGE and analyzed using ImageJ software. For control, nude Cu^{2+} -specific DNAzyme was prepared by hybridizing Enzyme-1 and Substrate-1 in a 1:1 and incubated in 1 μM concentration in 5 U/L DNase I or 50% cell lysate at the same conditions.

2.6. Cell Viability

The cytotoxicity of the FNAzymes was evaluated by an MTT assay. HeLa cells were seeded in a 96-well plate at a concentration of 1×10^5 cells per well. The plates were allowed to maintain in an air incubator containing 5% CO_2 /95% air at 37 °C for 24 h and then rinsed with fresh medium. Different concentrations of FNAzymes (0, 1, 3, 5, 10, 20, 50, 80, 160, and 320 nM) were added for another 24 h incubation, followed by the addition of 0.5 mg/mL MTT (final concentration). Four hours later, the media containing MTT was discarded by washing. The DMSO (150 μL) was then introduced to dissolve the formazan crystals in each well. The absorbance at 490 nm was recorded using a microplate reader (EL \times 808, BioTek, Winooski, VT, USA) for the final product.

2.7. Confocal Fluorescence Imaging

HeLa cells were incubated in a cell culture dish (MatTek, Ashland, MA, USA) with 1.0×10^5 cells per well. Certain amounts of Cu^{2+} and Zn^{2+} were added to each well for a 1 h incubation and then washed with PBS buffer three times. Then, 50 nM of FNAzymes were diluted in fresh medium and introduced for a 3 h incubation at 37 °C, followed by washing with PBS buffer three times. Images were monitored using an FV1000 LSCM (Olympus Optical Co., Ltd., Tokyo, Japan) with various laser transmitters.

2.8. Flow Cytometric Assay

HeLa cells were first treated with various concentrations of Cu^{2+} or Zn^{2+} (100, 200, 800, 3000, and 5000 nM) for 1 h, followed by incubating with 50 nM FNAzymes for another 3 h and washing with PBS buffer three times. Afterward, the HeLa cells were trypsinized and suspended in a new medium. The fluorescence intensity was analyzed using a BD FACSCanto flow cytometer (Merck Millipore, Darmstadt, Germany) in real time. The fluorescence intensities of FAM and ROX were obtained by 488 nm and 561 nm excitation, respectively.

2.9. Inductively Coupled Plasma-Mass Spectrometer (ICP-MS) Test

For the inductively coupled plasma-mass Spectrometer (ICP-MS) test, the trypsinized cells were counted with a cell counter and then transferred to a centrifuge tube and collected by centrifugation. After being dealt with aqua regia (3:1 hydrochloric acid/nitric acid, 200 μL) for 12 h, the cells were treated with ultrasound for 30 min to fully dissolve the two kinds of metal elements for the ICP-MS analysis (NexION 300D, PerkinElmer, Waltham, MA, USA). The concentrations of the two metal ions inside cells were calculated from the result of ICP-MS detection.

3. Results and Discussion

3.1. Simultaneous Detection of Cu^{2+} and Zn^{2+} In Vitro

As illustrated in Figure 1A, four strands (S1, S2, S3, and S4) containing Cu^{2+} -specific DNAzyme (marked in green on S3 and S4), Zn^{2+} -specific DNAzyme (marked in yellow on S1 and S2), fluorophores (FAM and ROX), and quenchers (Dabcyl and BHQ-2) are self-assembled into a multifunctional FNAzyme by rapid thermal annealing. The formation of a well-defined tetrahedral nanostructure brought the fluorophore and quencher together; thus, the fluorescence of FAM and ROX was efficiently quenched by Dabcyl and BHQ-2, respectively. In the presence of Cu^{2+} and Zn^{2+} , specific cleavage sites can be identified, and the site of an adenine ribonucleotide (rA) can be cleaved. Therefore, the fluorophore-labeled portions of the substrate strands (S1 and S4) were released, and the corresponding fluorescence was recovered.

The formation of FNAzymes was first determined by 8% native PAGE (Figure S1). The relatively low mobility in band 1 suggested that a yield of over 90% of the nanostructure was successfully formed with a single thermal annealing step. The monodispersed DNA structure could be observed under AFM imaging (Figure S2). The feasibility of FNAzymes in simultaneously responding to Cu^{2+} and Zn^{2+} in vitro was evaluated by fluorescence measurement (Figure 2A,B). The well-defined nanostructure of FNAzymes brought the fluorophores (FAM and ROX) quite close to the quenching molecules (DABCYL and BHQ-2), resulting in high fluorescence quenching efficiency. In this state, the fluorescence of fluorophores could not be detected (curve a colored gray in Figure 2A,B). In the presence of 400 nM Cu^{2+} and Zn^{2+} , the observed fluorescence intensity of FAM at 520 nm (excited at 494 nm, curve b in Figure 2A) and ROX at 605 nm (excited at 580 nm, curve b in Figure 2B) was significantly increased, suggesting that the cleavage of rA sites by target metal ions caused the release of fluorophore-labeled substrate strands (S4 and S1 in Figure 2) and the recovery of fluorescence. Kinetic studies in Figure 2C,D indicated that the FNAzymes respond rapidly to the target Cu^{2+} and Zn^{2+} within 20 min, suggesting that the FNAzymes were able to respond to the target Cu^{2+} and Zn^{2+} with a fast response. Considering the fact that the change in fluorescence intensity is proportional to the change in concentration at low concentrations ($\Delta F = k\Delta c$), we measured fluorescence intensities to calculate the cleavage ratio of probes. Fluorescence change (ΔF) was calculated as the fluorescence following cleavage (signal) minus the fluorescence prior to cleavage (background). To test the ratio and rate of the cleavage, FNAzymes with 50 nM free FAM or 50 nM free ROX were assembled to simulate 100% cleavage. In detail, 50 nM FNAzymes-1 were assembled by 50 nM S1, S2, S3, and S4-2 (without FAM labeling). In order to simulate 100% cleavage, an amount of 50 nM of FAM-labeled DNA (F1) was added. The fluorescence at 520 nm was recorded, and the $\Delta F_{520 \text{ nm}}$ was calculated to be 98.2, while the $\Delta F_{520 \text{ nm}}$ in the presence of 400 nM Cu^{2+} was 23.8 (20 min incubation), indicating ~24.2% cleavage ratio of Cu^{2+} -responsive DNAzyme (Figure S3). Similarly, 50 nM FNAzymes-2 were assembled by 50 nM S1-2 (without ROX labeling), S2, S3, and S4. To simulate 100% cleavage, an amount of 50 nM of ROX-labeled DNA (F2) was added. The fluorescence at 605 nm was recorded, and the $\Delta F_{605 \text{ nm}}$ was calculated to be 103.1, while the $\Delta F_{605 \text{ nm}}$ in the presence of 400 nM Zn^{2+} was 32.4 (20 min incubation), indicating ~34.4% cleavage ratio of Zn^{2+} -responsive DNAzyme. The cleavage rates within the first 20 min were calculated to be 0.61 nM/min for Cu^{2+} -responded cleavage and 0.86 nM/min for Zn^{2+} -responded cleavage.

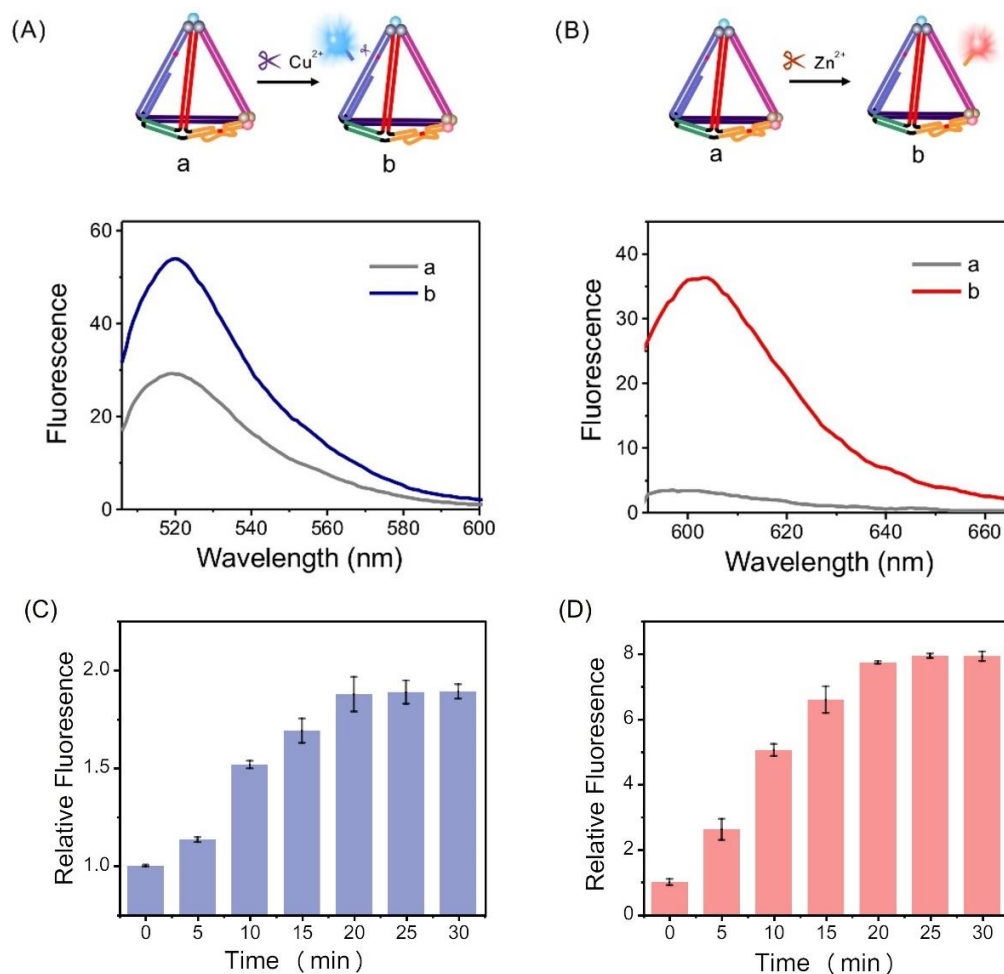


Figure 2. (A,B) Fluorescence response of the FNAzymes in the presence (a) or absence (b) of (A) 400 nM Cu^{2+} and (B) 400 nM Zn^{2+} . (C,D) Kinetics of the FNAzymes in the existence or absence of (C) 400 nM Cu^{2+} and (D) 400 nM Zn^{2+} . Cu^{2+} (FAM), $\lambda_{\text{ex}}/\lambda_{\text{em}}$: 494 nm/520 nm; Zn^{2+} (ROX), $\lambda_{\text{ex}}/\lambda_{\text{em}}$: 580 nm/605 nm.

Having demonstrated the feasibility of the simultaneous response of metal ions by FNAzymes, the detection sensitivity and selectivity in vitro were further tested. The observed FAM and ROX fluorescence increased gradually with the increase in concentrations of the target Cu^{2+} and Zn^{2+} (Figures 3 and S4), respectively, suggesting that the cleavage of DNAzyme by the corresponding target metal ions leads to fluorescence recovery. Strong linear correlations were observed between the maximum fluorescence intensities and the $\log C$ of the target metal ions ranging from 10 nM to 5000 nM with high correlation coefficients ($R^2 = 0.9905$ for Cu^{2+} and 0.9849 for Zn^{2+} , respectively). The detection limits of the FNAzymes for Cu^{2+} and Zn^{2+} were estimated to be 6.8 nM and 0.9 nM, respectively, indicating that the FNAzymes showed excellent detecting performance. The selectivity of FNAzymes was evaluated by detecting Cu^{2+} and Zn^{2+} in the presence of other relevant metal ions (Mn^{2+} , Li^+ , Ni^+ , Fe^{3+} , Cr^{2+} , and Co^{2+}) at a concentration of 1000 nM. A 3.3~11.7-fold enhancement in the fluorescence signal was observed for the target Cu^{2+} and Zn^{2+} compared to that for other ions (Figure S5). This indicated that DNAzymes could differentiate the target ions from others. However, the selectivity for the target metal ions was moderate or comparable as compared to other studies [32,33], which might be caused by the relatively low cleavage ratio of FNAzymes in the presence of metal ions and the relatively high background signal. Taken together, FNAzymes displayed good sensitivity and selectivity in vitro in signaling the Cu^{2+} and Zn^{2+} ions.

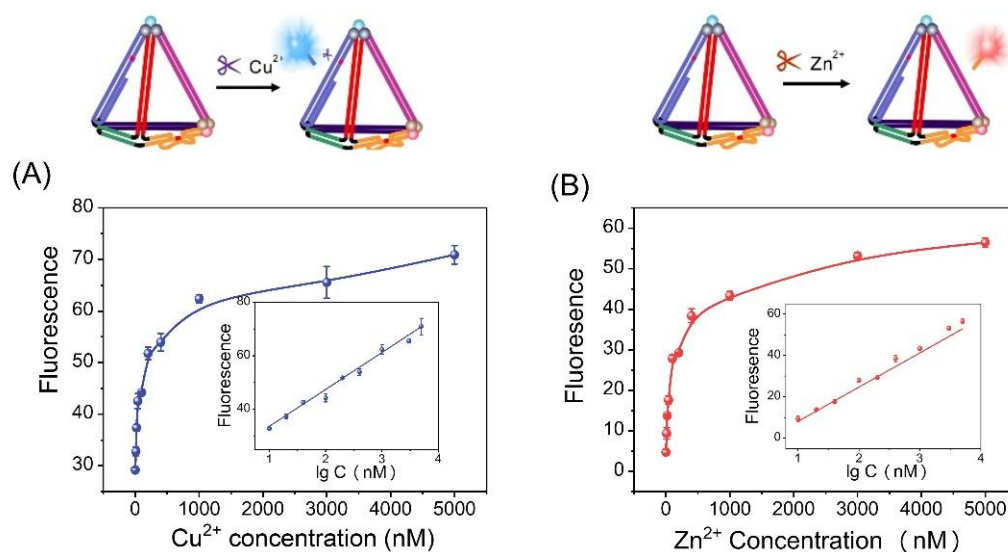


Figure 3. Plots of fluorescence peak intensities versus different concentrations of (A) Cu^{2+} and (B) Zn^{2+} . Insets are the corresponding calibration curve. Each experiment was repeated at least three times. Cu^{2+} (FAM), $\lambda_{\text{ex}}/\lambda_{\text{em}}$: 494 nm/520 nm; Zn^{2+} (ROX), $\lambda_{\text{ex}}/\lambda_{\text{em}}$: 580 nm/605 nm.

3.2. Stability and Cytotoxicity of the FNAzymes

Since the nanoprobe will be applied in a complex biological environment, the structural integrity of the FNAzymes was monitored in a DNase I solution and characterized with PAGE gel analysis. DNase I is a well-known endonuclease that efficiently digests single- or double-stranded DNA efficiently. From Figure 4A,B, a band of FNAzymes was visible for 12 h, indicating that the rigid structure was maintained against degradation by DNase I. As a control, the nude duplex Cu^{2+} -specific DNAzyme could not be visualized on PAGE gel after 8 h, indicating a much lower structural stability of the duplex structure. The enhanced stability of FNAzymes was in agreement with recently published data, which was attributed to the enzymatic resistance ability of rigid DNA nanostructures. These results further illustrated that the nude duplex DNAzyme could not work for a long time in the complex biological environment without protection due to its instability in cells [34,35]. Then, the stability of FNAzymes was further investigated in 50% cell lysate (human cervical cancer) and characterized by 8% PAGE gel analysis (Figure S6). The clear band observed after 12 h of incubation also demonstrates the good biostability of FNAzymes in cellular components. Within a period of three hours, it is possible that up to 80% of the structure would remain intact, allowing for semi-quantitative imaging in living cells. As a comparison, the nude duplex Cu^{2+} -specific DNAzyme was significantly degraded after four hours. Furthermore, the toxicity of the FNAzymes was evaluated by a standard colorimetric MTT assay. The HeLa cells were incubated with various concentrations of FNAzymes ranging from 0 to 320 nM at 37 °C for 24 h (Figure 4C). Even under the highest concentration at 320 nM, HeLa cells maintained high activity (>85%), indicating that the FNAzymes appeared to have no obvious toxicity or side effects on the living cells. With high stability in the cellular environment and low cellular cytotoxicity, the FNAzymes were applicable for intracellular detection of Cu^{2+} and Zn^{2+} .

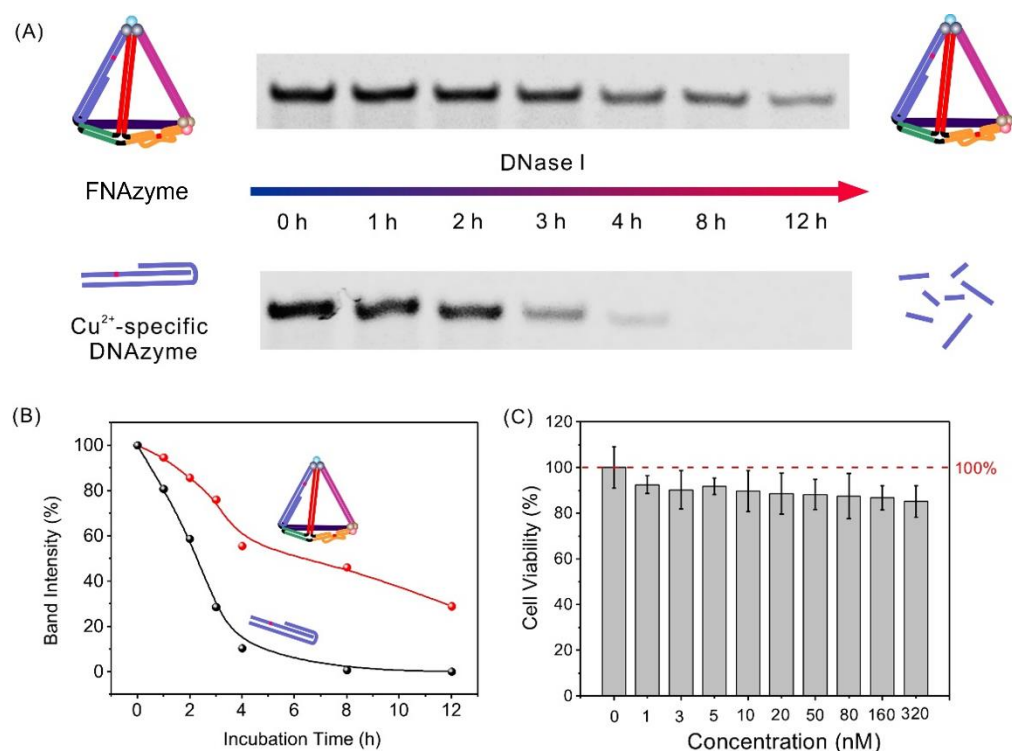


Figure 4. (A) Electrophoresis characterization for the stability of the FNAzymes (the upper row) and the nude Cu²⁺-dependent DNAzyme (the lower row) treated with 5 U/L DNase I at 37 °C from 0 to 12 h. The concentrations of probes are all 1 μM. (B) Band intensity of FNAzymes (red dots) and the nude Cu²⁺-dependent DNAzymes (black dots) after incubating with 5 U/L DNase I at 37 °C for different times in gel image (A). (C) Viability of HeLa cells incubated with various concentrations of FNAzymes for 24 h, respectively. Three experiments were conducted in each group, respectively.

3.3. Intracellular Imaging of Cu²⁺ and Zn²⁺ with FNAzymes

As demonstrated above, FNAzymes have the advantages of high sensitivity, high selectivity, fast detection speed, low cytotoxicity, and satisfactory stability in an intracellular environment. Hence, we aim to detect Cu²⁺ and Zn²⁺ in living cells using HeLa cells as the model. Firstly, HeLa cells without metal ion treatment were observed by confocal imaging. Under excitation of an appropriate voltage (590 V), almost no fluorescence signal was observed for cells that had not been treated with metal ions (Figure 5A). To verify that fluorescence was caused by metal ions in cells, HeLa cells were exposed to 5 μM Cu²⁺ or 5 μM Zn²⁺ for 1 h to enable the uptake of the metal ions, followed by incubation with FNAzymes for 3 h and observation through confocal imaging under the same experimental conditions. Cells incubated with Cu²⁺ ions showed bright green fluorescence (Figure 5B), while those incubated with Zn²⁺ ions exhibited red fluorescence (Figure 5C). Then, HeLa cells incubated with 5 μM Cu²⁺ and 5 μM Zn²⁺ were observed by confocal imaging. A bright green fluorescence signal for Cu²⁺ could be seen in the “FAM” channel under 480 nm excitation, and a red fluorescence signal for Zn²⁺ could be observed in the “ROX” channel under 559 nm excitation (Figure 5D). The bright-field images in Figure 5 indicated that HeLa cells were viable during the imaging process, while the overlap image confirms the simultaneous intracellular detections of Cu²⁺ and Zn²⁺. From the inductively coupled plasma-mass spectrometer (ICP-MS) results, the intracellular concentrations of Cu²⁺ and Zn²⁺ under the experimental conditions are estimated to be 101.12 nM and 96.22 nM, respectively (assuming 2000 μm³ as the volume of a cell) [22]. The results indicated that FNAzymes performed well in imaging Cu²⁺ and Zn²⁺ simultaneously in single living cells.

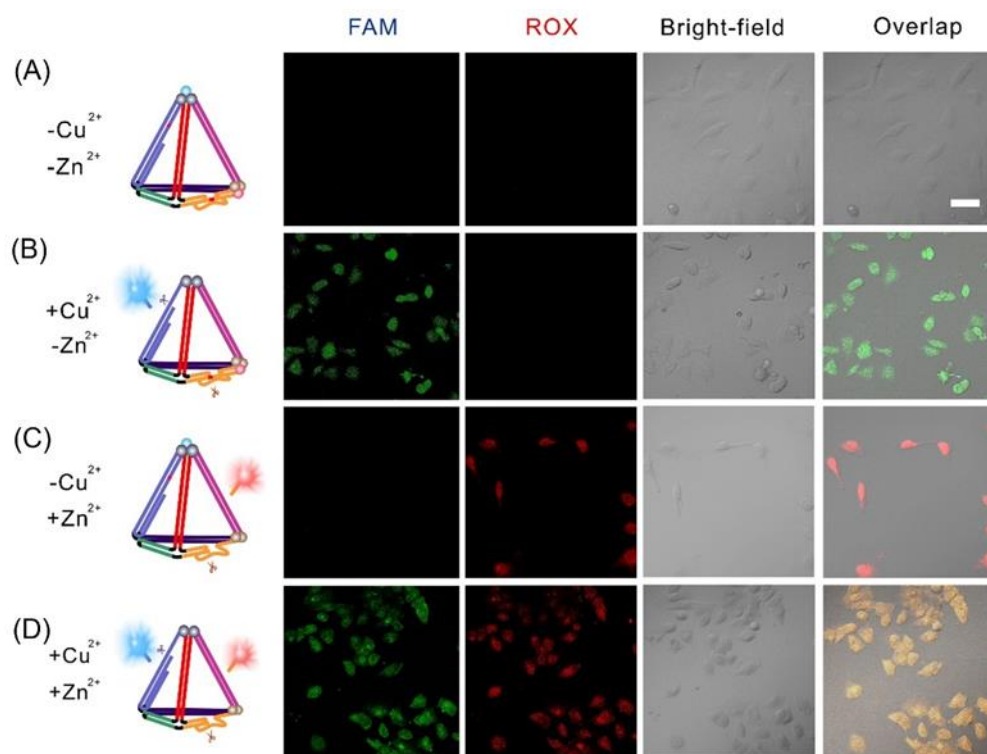


Figure 5. Fluorescence imaging of metal ions in living HeLa cells after treatment with (A) Cu^{2+} and Zn^{2+} ; (B) Cu^{2+} only; (C) Zn^{2+} only; or (D) no metal ions and incubated with FNAzymes. The green channel (the first row) is FAM fluorescence (λ_{ex} : 480 nm), and the red channel (the second row) is ROX fluorescence (λ_{ex} : 559 nm). Scale bar: 50 μm .

3.4. Semi-Quantitative Detection of Cu^{2+} and Zn^{2+} in Living Cells

To semi-quantitatively detect physiologically related metal ions in cells, analytical flow cytometry was employed to analyze the intracellular fluorescence intensity in a large population of cells. Different concentrations of Cu^{2+} and Zn^{2+} ranging from 0 to 5 μM were allowed to incubate with HeLa cells for 1 h, respectively. As the concentrations of metal ions in the cells increased, the signal intensity peak in flow cytometry shifted accordingly, which agreed with the corresponding fluorescence intensities observed in the confocal images (Figure 6A,B). The results indicated that FNAzymes could effectively monitor intracellular metal ions. The fluorescence signals were semi-quantified by the fluorescence intensities of the flow cytometry and the added concentrations of Cu^{2+} and Zn^{2+} (Figure 6C,D). An approximate linear relationship between fluorescence intensities and concentrations of added metal ions was observed. The excellent reproducibility of imaging sensitivity was proposed to be attributed to the high structural uniformity of FNAzymes, where signaling molecules were attached to FNAzymes at a 1:1 ratio with high precision. These results suggested that FNAzymes could be used as an effective tool for the semi-quantitative and simultaneous determination of intracellular metal ions.

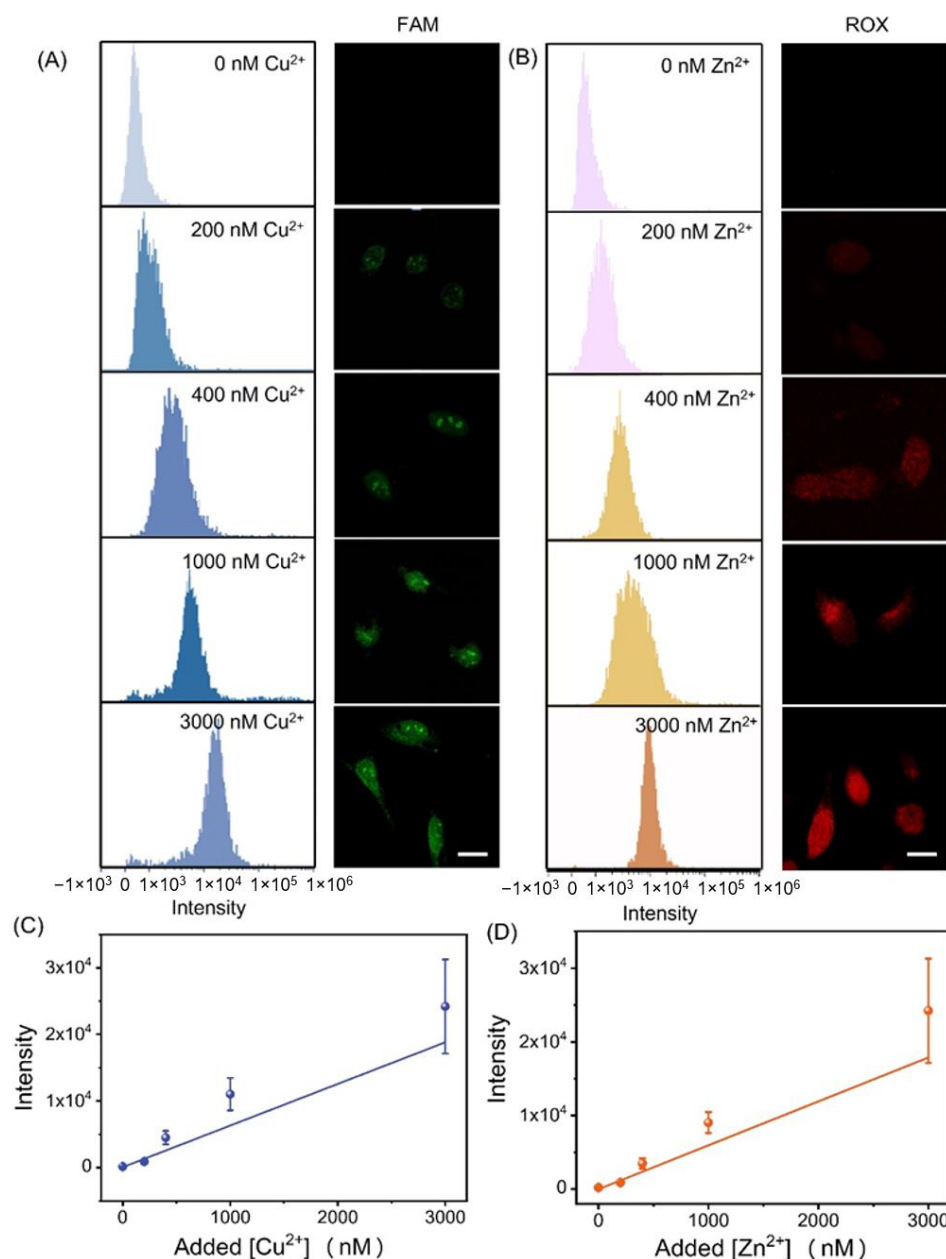


Figure 6. Semi-quantitative detection of intracellular Cu²⁺ and Zn²⁺ with FNAzymes. (A,B) Flow cytometry (left) and confocal images results (right) of HeLa cells incubated with 50 nM FNAzymes and different concentrations (0, 200, 400, 1000, and 3000 nM) of (A) Cu²⁺ and (B) Zn²⁺. Scale bar: 25 μ m. (C,D) Fluorescence intensity of the FNAzymes corresponding to various concentrations of added (C) Cu²⁺ and (D) Zn²⁺. Error bars represented standard deviations of at least three independent experiments.

4. Conclusions

In conclusion, we have proposed elaborate FNAzymes for the non-destructive simultaneous and quantitative detection of physiologically related Cu²⁺ and Zn²⁺ inside living cells by combining the highly active DNAzyme and DNA tetrahedron with good intracellular stability. As a promising nanocarrier for entering cells, FNAzymes with favorable biocompatibility can be easily prepared in one step with a high yield of over 90%, making them suitable for non-destructive intracellular detection. The excellent high structural uniformity endows FNAzymes with excellent and highly reproducible detection properties, which improve the accuracy of quantitative detection of intracellular ions. The excellent

high structural uniformity endows FNazymes with excellent and highly reproducible detection properties, which improve the accuracy of quantitative detection of intracellular ions. Due to the amplification effect of DNazymes, the assay displays low-nanomolar sensitivity for signaling Cu^{2+} and Zn^{2+} with a fast response time within 20 min. Enhancing the selectivity could be achieved by further designing a fluorescent probe with more efficient quenchers or fluorophores. We envision that this method could offer great opportunities for the quantitative detection of multiple targets in living cells and contribute to advancing our knowledge and understanding of the functions of Cu^{2+} and Zn^{2+} in biological research.

Supplementary Materials: The following supporting information can be downloaded at: <https://www.mdpi.com/article/10.3390/chemosensors11070358/s1>. Table S1: Sequences in the experiment; Figure S1: Native PAGE (8%) analysis of the self-assembled products; Figure S2: AFM image of the FNazymes; Figure S3: The Fluorescence change of FNazyme after metal ions-responded cleavage; Figure S4: Fluorescence spectra of the FNazymes with various concentrations of metal ions; Figure S5: Selectivity evaluation of the FNazymes; Figure S6: Electrophoresis characterization of the FNazymes and DNazymes incubated in 50% cell lysate.

Author Contributions: Conceptualization, D.Z. and L.W.; methodology, J.H. and S.S.; software, validation, and investigation, J.H. and Y.X.; resources, X.Z.; writing—original draft preparation, D.Z. and J.H.; writing—review and editing, D.Z. and Q.L.; supervision, X.Z. and L.W.; project administration, Q.L. and L.W.; funding acquisition, D.Z. and L.W. All authors have read and agreed to the published version of the manuscript.

Funding: This work was financially supported by the National Natural Science Foundation of China (62071251, 62235008, 62227803, 62288102), Natural Science Foundation of Jiangsu Province (BK20201376, BK20212012), “Belt and Road” Innovation Cooperation Project of Jiangsu (BZ2022011), Qinglan Project of Jiangsu Province of China, Young Scientific and Technological Talents Project of Jiangsu Association for Science and Technology (TJ-2021-028), and Project of State Key Laboratory of Organic Electronics and Information Displays, Nanjing University of Posts and Telecommunications (No. GZR2022010026).

Institutional Review Board Statement: Not applicable.

Informed Consent Statement: Not applicable.

Data Availability Statement: Not applicable.

Conflicts of Interest: The authors declare no conflict of interest. The funders had no role in the design of the study; in the collection, analyses, or interpretation of data; in the writing of the manuscript; or in the decision to publish the results.

References

1. Bolognin, S.; Messori, L.; Zatta, P. Metal ion physiopathology in neurodegenerative disorders. *Neuromol. Med.* **2009**, *11*, 223–238. [[CrossRef](#)] [[PubMed](#)]
2. Krezel, A.; Maret, W. The functions of metamorphic metallothioneins in zinc and copper metabolism. *Int. J. Mol. Sci.* **2017**, *18*, 1237. [[CrossRef](#)]
3. Winge, D.R.; Jensen, L.T.; Srinivasan, C. Metal-ion regulation of gene expression in yeast. *Curr. Opin. Chem. Biol.* **1998**, *2*, 216–221. [[CrossRef](#)] [[PubMed](#)]
4. Stelmashook, E.V.; Isaev, N.K.; Genrikhs, E.E.; Amelkina, G.A.; Khaspekov, L.G.; Skrebitsky, V.G.; Illarioshkin, S.N. Role of zinc and copper ions in the pathogenetic mechanisms of alzheimer’s and parkinson’s diseases. *Biochemistry* **2014**, *79*, 391–396. [[CrossRef](#)]
5. Krueger, W.H.H.; Gonye, G.E.; Madison, D.L.; Murray, K.E.; Kumar, M.; Spoerel, N.; Pfeiffer, S.E. Tpo1, a member of a novel protein family, is developmentally regulated in cultured oligodendrocytes. *J. Neurochem.* **1997**, *69*, 1343–1355. [[CrossRef](#)]
6. Islamoglu, Y.; Evliyaoglu, O.; Tekbas, E.; Cil, H.; Elbey, M.A.; Atilgan, Z.; Kaya, H.; Bilik, Z.; Akyuz, A.; Alan, S. The relationship between serum levels of Zn and Cu and severity of coronary atherosclerosis. *Biol. Trace Elem. Res.* **2011**, *144*, 436–444. [[CrossRef](#)] [[PubMed](#)]
7. Milne, A.; Landing, W.; Bizimis, M.; Morton, P. Determination of Mn, Fe, Co, Ni, Cu, Zn, Cd and Pb in seawater using high resolution magnetic sector inductively coupled mass spectrometry (HR-ICP-MS). *Anal. Chim. Acta* **2010**, *665*, 200–207. [[CrossRef](#)]
8. Cui, Y.; Chang, X.; Zhai, Y.; Zhu, X.; Zheng, H.; Lian, N. ICP-AES determination of trace elements after preconcentrated with p-dimethylaminobenzaldehyde-modified nanometer SiO_2 from sample solution. *Microchem. J.* **2006**, *83*, 35–41. [[CrossRef](#)]
9. Lin, P.H.; Danadurai, K.S.K.; Huang, S.D. Simultaneous determination of cobalt, nickel and copper in seawater with a multi-element electrothermal atomic absorption spectrometer and microcolumn preconcentration. *J. Anal. Atom. Spectrom.* **2001**, *16*, 409–412. [[CrossRef](#)]

10. Sheth, V.; Chen, X.; Mettenbrink, E.M.; Yang, W.; Jones, M.A.; M'Saad, O.; Thomas, A.G.; Newport, R.S.; Francek, E.; Wang, L.; et al. Quantifying intracellular nanoparticle distributions with three-dimensional super-resolution microscopy. *ACS Nano* **2023**, *17*, 8376–8392. [[CrossRef](#)]
11. Wang, S.; Deng, S.; Cai, X.; Hou, S.; Li, J.; Gao, Z.; Li, J.; Wang, L.; Fan, C. Superresolution imaging of telomeres with continuous wave stimulated emission depletion (STED) microscope. *Sci. China Chem.* **2016**, *59*, 1519–1524. [[CrossRef](#)]
12. Bao, L.; Ding, L.; Hui, J.; Ju, H. A light-up imaging protocol for neutral pH-enhanced fluorescence detection of lysosomal neuraminidase activity in living cells. *Chem. Commun.* **2016**, *52*, 12897–12900. [[CrossRef](#)]
13. Li, B.; Kou, J.; Mei, H.; Gu, X.; Wang, M.; Xie, X.; Xu, K. A hemicyanine-based “turn-on” fluorescent probe for the selective detection of Cu²⁺ ions and imaging in living cells. *Anal. Methods-UK* **2020**, *12*, 4181–4184. [[CrossRef](#)]
14. Zhang, X.; Song, Z.; Chao, Q.; Li, Q.; Kong, R.; Fan, G.; Luo, X. A DNAzyme-based normalized fluorescence strategy for direct quantification of endogenous zinc in living cells. *Chem. Commun.* **2022**, *58*, 577–580. [[CrossRef](#)]
15. Patil, M.; Keshav, K.; Kumawat, M.K.; Bothra, S.; Sahoo, S.K.; Srivastava, R.; Rajput, J.; Bendre, R.; Kuwar, A. Monoterpenoid derivative based ratiometric fluorescent chemosensor for bioimaging and intracellular detection of Zn²⁺ and Mg²⁺ ions. *J. Photoch. Photobio. A* **2018**, *364*, 758–763. [[CrossRef](#)]
16. Chen, Y.; Qiu, D.; Zhang, X.; Liu, Y.; Cheng, M.; Lei, J.; Mergny, J.; Ju, H.; Zhou, J. Highly sensitive biosensing applications of a magnetically immobilizable covalent G-quadruplex-hemin DNAzyme catalytic system. *Anal. Chem.* **2022**, *94*, 2212–2219. [[CrossRef](#)]
17. Guo, Y.; Chen, J.; Cheng, M.; Monchaud, D.; Zhou, J.; Ju, H. A thermophilic tetramolecular G-quadruplex/hemin DNAzyme. *Angew. Chem. Int. Ed.* **2017**, *56*, 16636–16640. [[CrossRef](#)] [[PubMed](#)]
18. McGhee, C.E.; Loh, K.Y.; Lu, Y. DNAzyme sensors for detection of metal ions in the environment and imaging them in living cells. *Curr. Opin. Biotech.* **2017**, *45*, 191–201. [[CrossRef](#)]
19. Wang, Q.; Wang, Z.; He, Y.; Xiong, B.; Li, Y.; Wang, F. Chemical and structural modification of RNA-cleaving DNAzymes for efficient biosensing and biomedical applications. *Trac-Trend Anal. Chem.* **2023**, *159*, 116910. [[CrossRef](#)]
20. Hu, L.; Fu, X.; Kong, G.; Yin, Y.; Meng, H.-M.; Ke, G.; Zhang, X.-B. DNAzyme-gold nanoparticle-based probes for biosensing and bioimaging. *J. Mater. Chem. B* **2020**, *8*, 9449–9465. [[CrossRef](#)]
21. Khan, S.; Burciu, B.; Filipe, C.D.M.; Li, Y.; Dellinger, K.; Didar, T.F. DNAzyme-based biosensors: Immobilization strategies, applications, and future prospective. *ACS Nano* **2021**, *15*, 13943–13969. [[CrossRef](#)] [[PubMed](#)]
22. Wu, P.; Hwang, K.; Lan, T.; Lu, Y. A DNAzyme-gold nanoparticle probe for uranyl ion in living cells. *J. Am. Chem. Soc.* **2013**, *135*, 5254–5257. [[CrossRef](#)] [[PubMed](#)]
23. Gerber, P.P.; Donde, M.J.; Matheson, N.J.; Taylor, A.I. XNAzymes targeting the SARS-CoV-2 genome inhibit viral infection. *Nat. Commun.* **2022**, *13*, 6716. [[CrossRef](#)]
24. Ge, Z.; Li, Q.; Fan, C. Framework nucleic acids for cell imaging and therapy. *Chem. Res. Chin. Univ.* **2020**, *36*, 1–9. [[CrossRef](#)]
25. Ge, Z.; Gu, H.; Li, Q.; Fan, C. Concept and development of framework nucleic acids. *J. Am. Chem. Soc.* **2018**, *140*, 17808–17819. [[CrossRef](#)]
26. Liu, Q.; Ge, Z.; Mao, X.; Zhou, G.; Zuo, X.; Shen, J.; Shi, J.; Li, J.; Wang, L.; Chen, X.; et al. Valency-controlled framework nucleic acid signal amplifiers. *Angew. Chem. Int. Ed.* **2018**, *57*, 7131–7135. [[CrossRef](#)]
27. Zhou, X.; Zhao, M.; Duan, X.; Guo, B.; Cheng, W.; Ding, S.; Ju, H. Collapse of DNA tetrahedron nanostructure for “off-on” fluorescence detection of DNA methyltransferase activity. *ACS Appl. Mater. Interfaces* **2017**, *9*, 40087–40093. [[CrossRef](#)] [[PubMed](#)]
28. Qing, Z.H.; Hu, J.L.; Xu, J.Y.; Zou, Z.; Lei, Y.L.; Qing, T.P.; Yang, R.H. An intramolecular catalytic hairpin assembly on a DNA tetrahedron for mRNA imaging in living cells: Improving reaction kinetics and signal stability. *Chem. Sci.* **2020**, *11*, 1985–1990. [[CrossRef](#)]
29. Liang, L.; Li, J.; Li, Q.; Huang, Q.; Shi, J.; Yan, H.; Fan, C. Single-particle tracking and modulation of cell entry pathways of a tetrahedral DNA nanostructure in live cells. *Angew. Chem. Int. Ed.* **2014**, *53*, 7745–7750. [[CrossRef](#)]
30. Liu, J.; Lu, Y. A DNAzyme catalytic beacon sensor for paramagnetic Cu²⁺ ions in aqueous solution with high sensitivity and selectivity. *J. Am. Chem. Soc.* **2007**, *129*, 9838–9839. [[CrossRef](#)]
31. Endo, M.; Takeuchi, Y.; Suzuki, Y.; Emura, T.; Hidaka, K.; Wang, F.; Willner, I.; Sugiyama, H. Single-molecule visualization of the activity of a Zn²⁺-dependent DNAzyme. *Angew. Chem. Int. Ed.* **2015**, *54*, 10550–10554. [[CrossRef](#)] [[PubMed](#)]
32. Ning, P.; Jiang, J.; Li, L.; Wang, S.; Yu, H.; Feng, Y.; Zhu, M.; Zhang, B.; Yin, H.; Guo, Q.; et al. A mitochondria-targeted ratiometric two-photon fluorescent probe for biological zinc ions detection. *Biosens. Bioelectron.* **2016**, *77*, 921–927. [[CrossRef](#)] [[PubMed](#)]
33. Su, M.; Liu, C.; Zhang, Y.; Rong, X.; Wang, X.; Li, X.; Wang, K.; Zhu, H.; Zhu, B. Rational design of a water-soluble TICT-AIEE-active fluorescent probe for mercury ion detection. *Anal. Chim. Acta* **2022**, *1230*, 340337. [[CrossRef](#)] [[PubMed](#)]
34. Li, F.; Liu, Y.; Dong, Y.; Chu, Y.; Song, N.; Yang, D. Dynamic assembly of DNA nanostructures in living cells for mitochondrial interference. *J. Am. Chem. Soc.* **2022**, *144*, 4667–4677. [[CrossRef](#)] [[PubMed](#)]
35. Lv, M.; Wu, Z.; Yu, R.; Jiang, J. Three-dimensional DNA nanostructures for dual-color microRNA imaging in living cells via hybridization chain reaction. *Chem. Commun.* **2020**, *56*, 6668–6671. [[CrossRef](#)] [[PubMed](#)]

Disclaimer/Publisher’s Note: The statements, opinions and data contained in all publications are solely those of the individual author(s) and contributor(s) and not of MDPI and/or the editor(s). MDPI and/or the editor(s) disclaim responsibility for any injury to people or property resulting from any ideas, methods, instructions or products referred to in the content.